J. Fluid Mech. (1971), *vol.* 49, *part* 1, *pp.* 33–48
Printed in Great Britain

The effect of sinusoidal protrusions on laminar free convection between vertical walls

By A. WATSON AND G. POOTS
Department of Applied Mathematics, University of Hull

(Received 21 July 1970 and in revised form 10 March 1971)

The effects of sinusoidal protrusions on steady laminar free convection between vertical walls is investigated in this paper. Numerical results are presented for various values of the size and spacing of the protrusions. In particular optimum values are found which yield maximum wall heat-transfer coefficients.

1. Introduction

One of the major problems occurring in the design of oil or gas-fired boilers is the realization of the optimum efficiency of the heat-transfer process under specified external conditions. Increases in the rate of heat transfer of such systems may be effected, as in common practice, by the attachment of fins, studs or other suitable protrusions to the wall of the boiler. The choice of such a simple expedient, however, raises the following question. What are the optimum values of the size and spacing of the protrusions? A complete answer to the above questions would involve many aspects of the particular heating system chosen but, nevertheless, gives some motivation to the present theoretical investigation.

The problem to be considered is that of the motion which occurs when a fluid is contained between two corrugated walls, the surfaces of which are maintained at constant, but dissimilar, temperatures T_0 and T_1. Specifically attention will be given to sinusoidal walls defined by

$$y = \pm d\{1 + \epsilon \sin(\omega x/d)\}, \tag{1.1}$$

where the axes of x and y are as given in figure 1.

The parameters ϵ and ω are a measure of the height and spacing of the protrusions; their amplitude and wavelength being ϵd and $2\pi d/\omega$ respectively.

It is supposed that the convective motion is two-dimensional and that the flow is laminar. It will be further supposed that the cavity between the walls is of sufficient extent for the flow to be assumed to be fully developed and periodic in the x direction.

This flow, in which the fluid rises up the hot wall and falls down the cool wall does not, of course, simulate the physical situation of a cooled up-flow occurring in the heating section of a boiler. Instead the above model is useful in a theoretical investigation into the effects of protrusions on a flow whose characteristics are known *a priori*. This particular flow configuration, in fact the case $\epsilon = 0$, corresponds to the flow between plane vertical walls and has been studied extensively

by Ostrach (1964). In this fully developed counterflow heat is transferred across the gap by conduction alone and the motion is entirely controlled by a balance of the viscous and buoyancy forces.

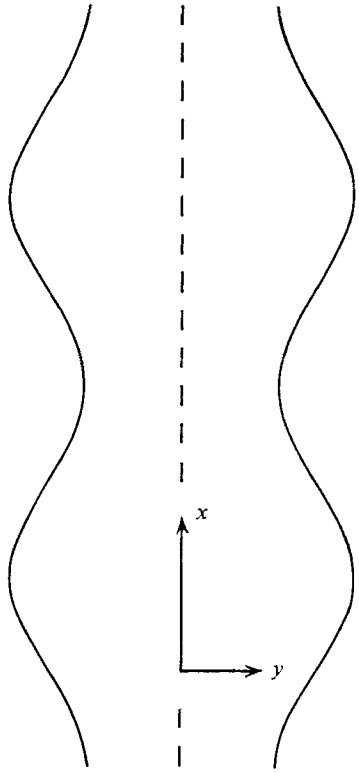

FIGURE 1. Geometrical configuration.

2. Analysis

Following Boussinesq (1903) the equations governing steady free convection are simplified by assuming that: (i) The temperature difference $T-T_m$ is small compared with the absolute temperature T_m, which is taken to be the mean of the wall temperatures T_0 and T_1. (ii) All physical constants of the gas are independent of the temperature and allowance is made for variations in density only in the calculation of the body force. (iii) The fluid is incompressible and viscous heat dissipation may be neglected.

If u and v denote the vertical and horizontal velocity components in the x and y directions, the equations expressing conservation of mass, momentum and energy are:

$$\frac{\partial u}{\partial x}+\frac{\partial v}{\partial y}=0, \tag{2.1}$$

$$u\frac{\partial u}{\partial x}+v\frac{\partial u}{\partial y}=-\frac{1}{\rho}\frac{\partial p}{\partial x}+\nu\nabla^2 u+g\frac{T-T_m}{T_m}, \tag{2.2}$$

$$u\frac{\partial v}{\partial x}+v\frac{\partial v}{\partial y}=-\frac{1}{\rho}\frac{\partial p}{\partial y}+\nu\nabla^2 v, \tag{2.3}$$

and

$$u\frac{\partial T}{\partial x}+v\frac{\partial T}{\partial y}=k\nabla^2 T. \tag{2.4}$$

Here ρ is the density, ν the kinematic viscosity and k the thermal diffusivity, all evaluated at the reference temperature T_m. p is the dynamic pressure and is the difference between the actual pressure and the hydrostatic pressure (in the absence of heating). Consequently, on employing the equation of state for a gas

$$\frac{\rho-\rho_m}{\rho_m}=-\frac{T-T_m}{T_m}, \tag{2.5}$$

the buoyancy force term is as given on the right-hand side of (2.2).

The boundary conditions for the channel shown in figure 1 are

$$u=v=0, \quad T=T_1 \quad \text{at} \quad y=-d(1+\epsilon\sin(\omega x/d)), \tag{2.6}$$

$$u=v=0, \quad T=T_0 \quad \text{at} \quad y=d(1+\epsilon\sin(\omega x/d)). \tag{2.7}$$

Equations (2.1)–(2.4) may be expressed in non-dimensional form by the introduction of the following variables

$$X=\frac{x}{d}, \quad Y=\frac{y}{d}, \quad \theta=2\left(\frac{T-T_m}{T_1-T_0}\right). \tag{2.8}$$

We also define a dimensionless stream function ψ, with the aid of (2.1) by the relations

$$u=\frac{\nu}{d}\frac{\partial\psi}{\partial Y}, \quad v=-\frac{\nu}{d}\frac{\partial\psi}{\partial X}. \tag{2.9}$$

The equations of motion then become, on elimination of p,

$$\nabla^4\psi+\frac{\partial(\psi,\nabla^2\psi)}{\partial(X,Y)}+G\frac{\partial\theta}{\partial Y}=0 \tag{2.10}$$

and

$$\nabla^2\theta+P\frac{\partial(\psi,\theta)}{\partial(X,Y)}=0, \tag{2.11}$$

where $P=\nu/k$ is the Prandtl number and $G=(gd^3/\nu^2)(T_1-T_0)/(T_1+T_0)$ is a Grashof number based on half of the mean distance separating the walls.

The appropriate boundary conditions, for all X, are

$$\partial\psi/\partial X=\partial\psi/\partial Y=0, \quad \theta=\mp 1 \quad \text{at} \quad Y=\pm(1+\epsilon\sin(\omega X)). \tag{2.12}$$

It is convenient to introduce the following transformation of the independent variables.

$$\xi=X, \quad \eta=Y/[1+\epsilon\sin(\omega X)]. \tag{2.13}$$

This affords great simplification of the boundary conditions since the space between the corrugated walls is transformed into the region bounded by the two planes $\eta=\pm 1$, for all ξ.

Expansions of ψ and θ in powers of ϵ are a natural consequence of the above

transformation. Since the flow has been assumed fully developed the zeroth-order functions will be independent of ξ, and so we let

$$\psi = \psi_0(\eta) + \epsilon\psi_1(\xi,\eta) + \epsilon^2\psi_2(\xi,\eta) + \ldots, \tag{2.14}$$

and

$$\theta = \theta_0(\eta) + \epsilon\theta_1(\xi,\eta) + \epsilon^2\theta_2(\xi,\eta) + \ldots. \tag{2.15}$$

These expansions are inserted into the governing equations (2.10)–(2.12) and, after employing (2.13), coefficients of successive powers of ϵ are equated to zero.

Zeroth-order equations in ψ_0 and θ_0

These are governed by

$$d^4\psi_0/d\eta^4 + G\,d\theta_0/d\eta = 0, \tag{2.16}$$

and

$$d^2\theta_0/d\eta^2 = 0, \tag{2.17}$$

and are subject to the boundary conditions:

$$\psi_0 = d\psi_0/d\eta = 0, \quad \theta_0 = \mp 1 \quad \text{at} \quad \eta = \pm 1, \quad \text{for all} \quad \xi. \tag{2.18}$$

Their solutions are

$$\psi_0(\eta) = \tfrac{1}{24}G(\eta^2-1)^2 \quad \text{and} \quad \theta_0(\eta) = -\eta. \tag{2.19}$$

This implies that the velocities occurring in the flow between plane vertical walls are of the order of $gd^2(T_1-T_0)/\nu(T_1+T_0)$, giving a balance between the viscous and buoyancy forces as previously stated.

First-order equations in ψ_1 and θ_1

Equating terms of order ϵ yields, on employing (2.19), the following equations:

$$\begin{aligned}\nabla^4\psi_1 + G\eta\frac{\partial\psi_1}{\partial\xi} - \tfrac{1}{6}G(\eta^3-\eta)\frac{\partial}{\partial\xi}(\nabla^2\psi_1) \\ + G\frac{\partial\theta_1}{\partial\eta} = \tfrac{1}{6}G\sin(\omega\xi)\,[\omega^4\eta^2(\eta^2-1) - 4\omega^2(6\eta^2-1) + 18] \\ + \tfrac{1}{36}\omega G^2\cos(\omega\xi)\,(\eta^3-\eta)\,[\omega^2\eta^2(\eta^2-1) - 6\eta^2 + 2],\end{aligned} \tag{2.20}$$

and

$$\nabla^2\theta_1 - P\left[\frac{\partial\psi_1}{\partial\xi} + \tfrac{1}{6}G(\eta^3-\eta)\frac{\partial\theta_1}{\partial\xi}\right] = \omega^2\eta\sin(\omega\xi). \tag{2.21}$$

The relevant boundary conditions are

$$\psi_1 = \partial\psi_1/\partial\eta = \theta_1 = 0 \quad \text{at} \quad \eta = \pm 1, \quad \text{for all} \quad \xi. \tag{2.22}$$

Intuitively the flow may be assumed to be periodic in the x direction, which is equivalent to supposing that the flow can be analyzed as a Fourier series in that direction. It suffices to let

$$\psi_1 = f_1(\eta)\sin(\omega\xi) + f_2(\eta)\cos(\omega\xi) \tag{2.23}$$

and

$$\theta_1 = g_1(\eta)\sin(\omega\xi) + g_2(\eta)\cos(\omega\xi). \tag{2.24}$$

The resultant amplitudes, f_j and g_j, satisfy the equations

$$L_1(D,\omega,G,f_j,g_j) = \tfrac{1}{6}G[\omega^4\eta^2(\eta^2-1) - 4\omega^2(6\eta^2-1) + 18], \tag{2.25}$$

$$L_2(D,\omega,G,f_j,g_j) = \tfrac{1}{36}\omega G^2(\eta^3-\eta)\,[\omega^2\eta^2(\eta^2-1) - 6\eta^2 + 2], \tag{2.26}$$

$$M_1(D,\omega,G,f_j,g_j) = \omega^2\eta, \tag{2.27}$$

and

$$M_2(D,\omega,G,f_j,g_j) = 0, \tag{2.28}$$

where D denotes the differential operator $d/d\eta$. The boundary conditions are

$$f_j(\pm 1) = Df_j(\pm 1) = g_j(\pm 1) = 0. \tag{2.29}$$

This system constitutes a twelfth-order boundary-value problem since the homogeneous parts of the equation are given by

$$L_1 = (D^2-\omega^2)^2 f_1 - \omega G\eta f_2 + GDg_1 + \tfrac{1}{6}\omega G(\eta^3-\eta)(D^2-\omega^2)f_2, \tag{2.30}$$

$$L_2 = (D^2-\omega^2)^2 f_2 + \omega G\eta f_1 + GDg_2 - \tfrac{1}{6}\omega G(\eta^3-\eta)(D^2-\omega^2)f_1, \tag{2.31}$$

$$M_1 = (D^2-\omega^2)g_1 + \omega P(f_2 + \tfrac{1}{6}G(\eta^3-\eta)g_2), \tag{2.32}$$

and

$$M_2 = (D^2-\omega^2)g_2 - \omega P(f_1 + \tfrac{1}{6}G(\eta^3-\eta)g_1). \tag{2.33}$$

The amplitudes f_j and g_j will, of course, be indeterminate if there exist eigensolutions of the coupled system

$$L_j = M_j = 0, \tag{2.34}$$

which satisfy boundary conditions (2.29). The existence of eigensolutions of (2.34) has been verified numerically and these indicate a lowest critical $(\omega - G)$ relation of the form

$$F(\omega, G) = 0. \tag{2.35}$$

In practice the critical values would also be expected to depend on the amplitude, as well as the frequency, of the corrugations. Such behaviour would most likely occur when $\epsilon = O(1)$ and may be assumed negligible for sufficiently small ϵ.

For values of ω and G in the neighbourhood of (2.35) the first-order corrections will predict large increases in velocity and heat transfer; clearly this situation is unacceptable from a physical viewpoint.

When (2.35) is satisfied the first-order terms become singular and these singularities will be propagated into the higher-order terms. Consequently the problem is then one of singular perturbation theory and the critical values correspond to a discontinuous transition from one mode of flow and heat transfer to another. Due to the complexity of the basic equations both numerical and singular perturbations approaches seem intractable.

The failure of the expansion in the present analysis may be taken to indicate the presence of an unstable flow régime. In fact the critical relation (2.35) also pertains to the problem of marginal stability of the convective flow between plane vertical walls, maintained at temperatures T_0 and T_1. The equations governing this flow are as given in (2.10) and (2.11) subject to the boundary conditions:

$$\partial\psi/\partial X = \partial\psi/\partial Y = 0, \quad \theta = \mp 1 \quad \text{at} \quad Y = \pm 1, \quad \text{all } X. \tag{2.36}$$

These yield the steady fully developed solution

$$\overline{\psi} = \tfrac{1}{24}G(Y^2-1)^2, \quad \overline{\theta} = -Y. \tag{2.37}$$

As is usual, in linear stability analysis, we set

$$\psi = \overline{\psi} + \psi^*, \quad \theta = \overline{\theta} + \theta^*. \tag{2.38}$$

Assuming that products of the disturbance components are negligible, the perturbation equations in ψ^* and θ^* reduce to

$$\nabla^*\psi^* + GY\frac{\partial\psi^*}{\partial X} - \frac{G}{6}(Y^3 - Y)\frac{\partial}{\partial X}(\nabla^2\psi^*) + G\frac{\partial\theta^*}{\partial Y} = 0, \tag{2.39}$$

and

$$\nabla^2\theta^* - P\left(\frac{\partial\psi^*}{\partial X} + \frac{G}{6}(Y^3 - Y)\frac{\partial\theta^*}{\partial X}\right) = 0. \tag{2.40}$$

The disturbance is now assumed to be periodic in the X direction and decomposition into normal modes yields

$$\psi^* = \psi_1(X, Y), \quad \theta^* = \theta_1(X, Y), \tag{2.41}$$

where ψ_1 and θ_1 are given by (2.23) and (2.24) and satisfy the homogeneous system (2.34) subject to the conditions given in (2.29). Thus, as previously stated, the critical values for marginal stability correspond to those evaluated in (2.35).

Second-order equations in ψ_2 and θ_2

Equating terms of order ϵ^2 gives

$$\begin{aligned}
&\nabla^4\psi_2 + G\eta\frac{\partial\psi_2}{\partial\xi} - \frac{G}{6}(\eta^3 - \eta)\left[\frac{\partial^3\psi_2}{\partial\xi^3} + \frac{\partial^3\psi_2}{\partial\xi\,\partial\eta^2}\right] + \left[\frac{\partial\psi_1}{\partial\xi} - \cos(\omega\xi)\omega\frac{G}{6}\eta^2(\eta^2 - 1)\right] \\
&\quad\times\left[\frac{\partial^3\psi_1}{\partial\xi^2\,\partial\eta} + \frac{\partial^2\psi_1}{\partial\eta^3} + \sin(\omega\xi)\frac{G}{3}\eta\{\omega^2(2\eta^2 - 1) - 9\}\right] \\
&\quad - \left[\frac{\partial\psi_1}{\partial\eta} - \sin(\omega\xi)\frac{G}{6}(\eta^3 - \eta)\right] \\
&\quad\times\left[\frac{\partial^3\psi_1}{\partial\xi^3} + \frac{\partial^3\psi_1}{\partial\xi\,\partial\eta^2} + \cos(\omega\xi)\omega\frac{G}{6}\{\omega^2\eta^2(\eta^2 - 1) - 2(6\eta^2 - 1)\}\right] \\
&\quad + \sin(\omega\xi)\left\{-4\frac{\partial^4\psi_1}{\partial\eta^4} - 4\frac{\partial^4\psi_1}{\partial\xi^2\,\partial\eta^2} + 2\omega^2\eta\left[\frac{\partial^3\psi_1}{\partial\eta^3} + 3\frac{\partial^3\psi_1}{\partial\xi^2\,\partial\eta}\right]\right. \\
&\quad \left. + 4\omega^2\frac{\partial^2\psi_1}{\partial\eta^2} - \omega^4\eta\frac{\partial\psi_1}{\partial\eta} + \frac{G}{6}(\eta^3 - \eta)\left[2\frac{\partial^3\psi_1}{\partial\xi\,\partial\eta^2} - 3\omega^2\eta\frac{\partial^2\psi_1}{\partial\xi\,\partial\eta}\right]\right\} \\
&\quad + \cos(\omega\xi)\left\{-4\omega\eta\left[\frac{\partial^4\psi_1}{\partial\xi^3\,\partial\eta} + \frac{\partial^4\psi_1}{\partial\xi\,\partial\eta^3}\right] - \omega G\eta^2\frac{\partial\psi_1}{\partial\eta} - 8\omega\frac{\partial^3\psi_1}{\partial\xi\,\partial\eta^2} + 4\omega^3\eta\frac{\partial^2\psi_1}{\partial\xi\,\partial\eta}\right. \\
&\quad \left. + \omega\frac{G}{6}\eta^2(\eta^2 - 1)\left[\frac{\partial^3\psi_1}{\partial\eta^3} + 3\frac{\partial^3\psi_1}{\partial\xi^2\,\partial\eta} - \omega^2\frac{\partial\psi_1}{\partial\eta}\right] + \omega\frac{G}{3}(\eta^3 - \eta)\frac{\partial^2\psi_1}{\partial\eta^2}\right\} \\
&\quad + \sin(2\omega\xi)\omega\frac{G^2}{12}(\eta^3 - \eta)\left\{\frac{\omega^2}{3}\eta^2(8\eta^2 - 5) - 5\eta^2 + 1\right\} \\
&\quad + \cos(2\omega\xi)\frac{G}{2}\left[-\frac{\omega^4}{3}\eta^2(18\eta^2 - 11) + 4\omega^2(8\eta^2 - 1) - 9\right] \\
&\quad + \frac{G}{2}\left[-\frac{\omega^4}{3}\eta^2(2\eta^2 - 1) + 8\omega^2\eta^2 + 9\right] + G\frac{\partial\theta_2}{\partial\eta} - \sin(\omega\xi)G\frac{\partial\theta_1}{\partial\eta} = 0,
\end{aligned} \tag{2.42}$$

and also

$$\nabla^2\theta_2 - P\frac{G}{6}(\eta^3-\eta)\frac{\partial\theta_2}{\partial\xi} - P\frac{\partial\psi_2}{\partial\xi} + P\left[\frac{\partial\theta_1}{\partial\eta}\frac{\partial\psi_1}{\partial\xi} - \frac{\partial\theta_1}{\partial\xi}\frac{\partial\psi_1}{\partial\eta}\right]$$
$$+\sin(\omega\xi)\left[\omega^2\eta\frac{\partial\theta_1}{\partial\eta} - 2\frac{\partial^2\theta_1}{\partial\eta^2} + P\frac{\partial\psi_1}{\partial\xi} + P\frac{G}{6}(\eta^3-\eta)\frac{\partial\theta_1}{\partial\xi}\right]$$
$$-\cos(\omega\xi)2\omega\eta\frac{\partial^2\theta_1}{\partial\xi\,\partial\eta} - \tfrac{3}{2}\omega^2\eta\cos(2\omega\xi) - \tfrac{1}{2}\omega^2\eta = 0. \tag{2.43}$$

The second-order perturbations, ψ_2 and θ_2, can be expressed as

$$\psi_2 = f_3(\eta) + f_4(\eta)\sin(2\omega\xi) + f_5(\eta)\cos(2\omega\xi), \tag{2.44}$$

$$\theta_2 = g_3(\eta) + g_4(\eta)\sin(2\omega\xi) + g_5(\eta)\cos(2\omega\xi), \tag{2.45}$$

where the f_j and g_j satisfy an eighteenth-order system of inhomogeneous linear equations. Note that the equation for $g_3(\eta)$ does not contain the other second-order functions and is given by

$$D^2g_3 - D^2g_1 - \tfrac{1}{2}(\omega^2\eta + \omega Pf_2)Dg_1 - \tfrac{1}{2}\omega P(f_2 + g_1Df_2 - g_2Df_1 - f_1Dg_2)$$
$$-\tfrac{1}{12}\omega PG(\eta^3-\eta)g_2 - \tfrac{1}{2}\omega^2\eta = 0, \tag{2.46}$$

to be solved subject to
$$g_3(\pm 1) = 0. \tag{2.47}$$

For brevity the equations governing the remaining second-order amplitudes will not be stated. However, an important feature of these equations is their singular behaviour for values of ω and G given by

$$F(2\omega, G) = 0. \tag{2.48}$$

Moreover, investigation of the singular behaviour of the higher-order perturbation equations yields, for the mth-order terms, the more general relation

$$F(m\omega, G) = 0. \tag{2.49}$$

The perturbation expansion, due to the complexity of further analysis, is truncated at this point.

3. Numerical solutions

The equations governing the first- and second-order amplitudes have been solved numerically for air ($P = 0{\cdot}72$) for various values of ω and G. Since these equations are linear the method of complementary functions may be employed, one particular integral and as many complementary functions as are necessary being found. The integration procedure used was Merson's modification of the Runge–Kutta process. Both these methods are described by Lance (1960, ch. 3).

Solutions have been obtained for values of ω in the range 0·5 to 2·0 and for values of G below 1000. No difficulty in performing the integrations was encountered except that they become more time consuming as G is increased. The method of complementary functions breaks down at a critical point and this provides a suitable criterion for their determination; the results are displayed in table 1.

Some of the figures shown here were produced on the line printer of the computer. Each function to be displayed is first scaled so that it lies in the range 0 to 10. Contour bands, correct to the nearest integer, are then plotted with odd values being shaded by the appropriate digit and even values being left blank for clarity.

ω	0·50	0·75	1·00	1·25	1·40 (min)	1·50	1·75
G	1050·7	726·1	579·6	513·6	502·1	507·1	605·2

TABLE 1. Critical $(\omega - G)$ values

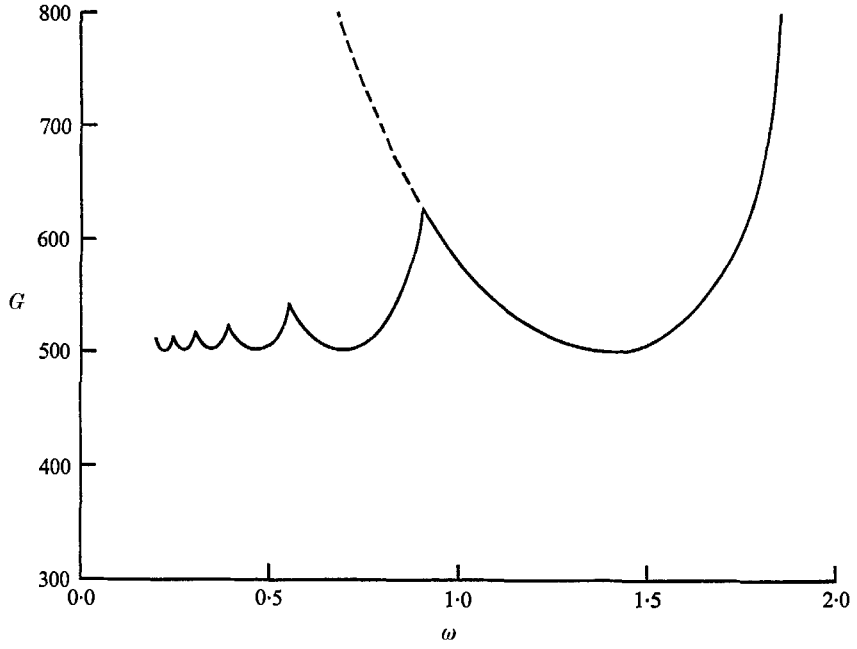

FIGURE 2. Critical $(\omega - G)$ values.

4. Results and discussion

It has been established that the minimum critical Grashof number of flow between corrugated walls of small amplitude occurs at $G = 502{\cdot}1$ with $\omega = 1{\cdot}40$ which, as shown in §2, correspond to the critical values for marginal stability between plane vertical walls. Vest & Arpaci (1969), in a recent investigation on the stability of natural convection in a vertical slot, have shown that, for the relevant conduction régime, the critical values for marginal stability are $\omega = 1{\cdot}33$ and $G = 492{\cdot}5$†. Their method of solution entailed the replacement of ψ and θ by truncated series of orthogonal functions. The values quoted in the present paper

† Note that in the work of Vest & Arpaci (1969) their wave-number, in our notation, is 2ω and their Grashof number is $16G$.

were found as a result of direct numerical integration of the first-order perturbation equations and are believed to be more reliable.

The perturbation expansion in the present problem yields critical curves of the form

$$F(m\omega, G) = 0 \quad (m = 1, 2, \ldots),$$

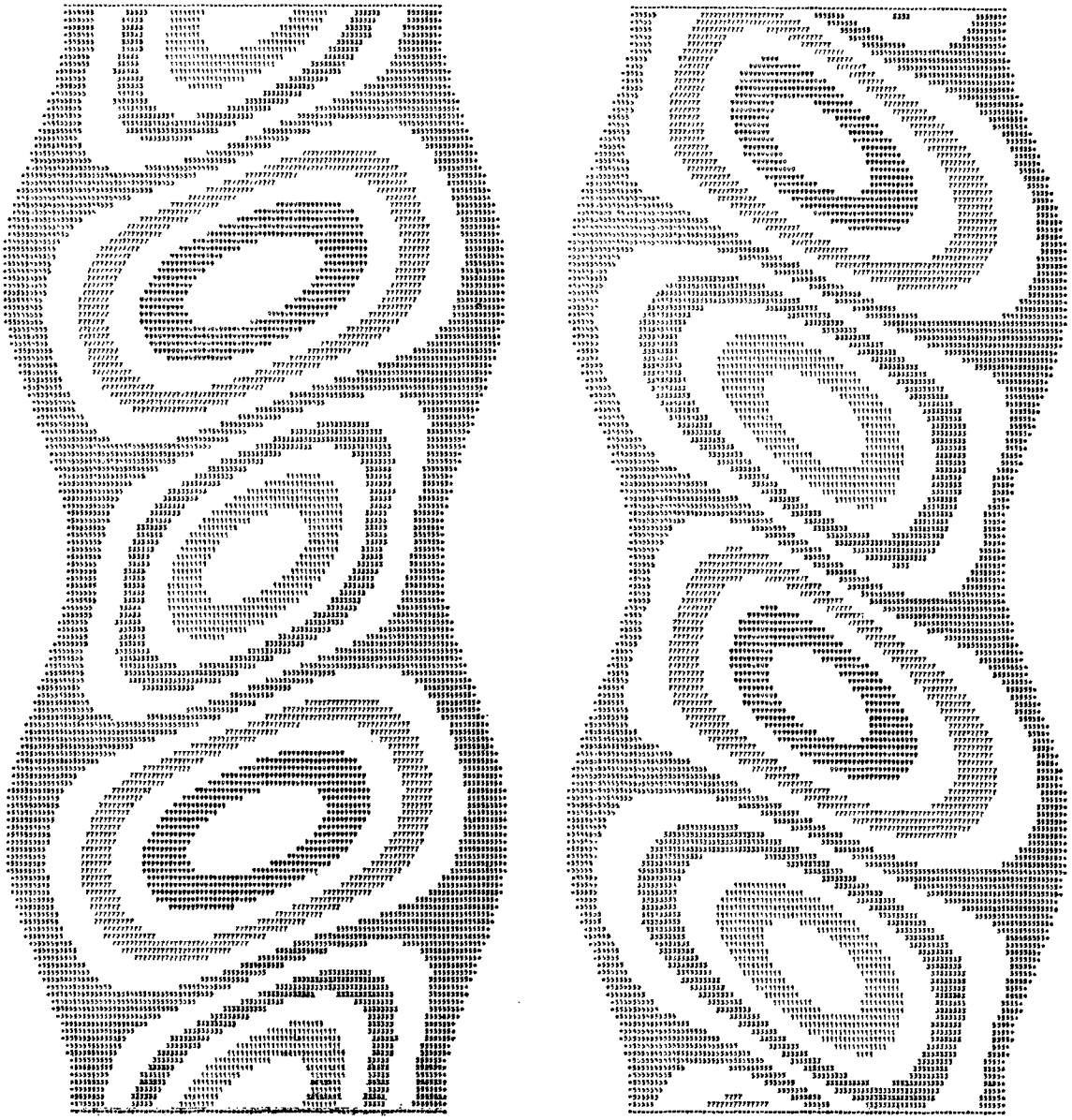

(*a*) (*b*)

FIGURE 3. (*a*) ψ_1 plot and (*b*) θ_1 plot for $\omega = 1{\cdot}5$ and $G = 200$.

which indicate the possible existence of instabilities in the flow for values of ω and G above the union of these curves (see figure 2). For this reason a description of the numerical results will be confined to the region below this curve.

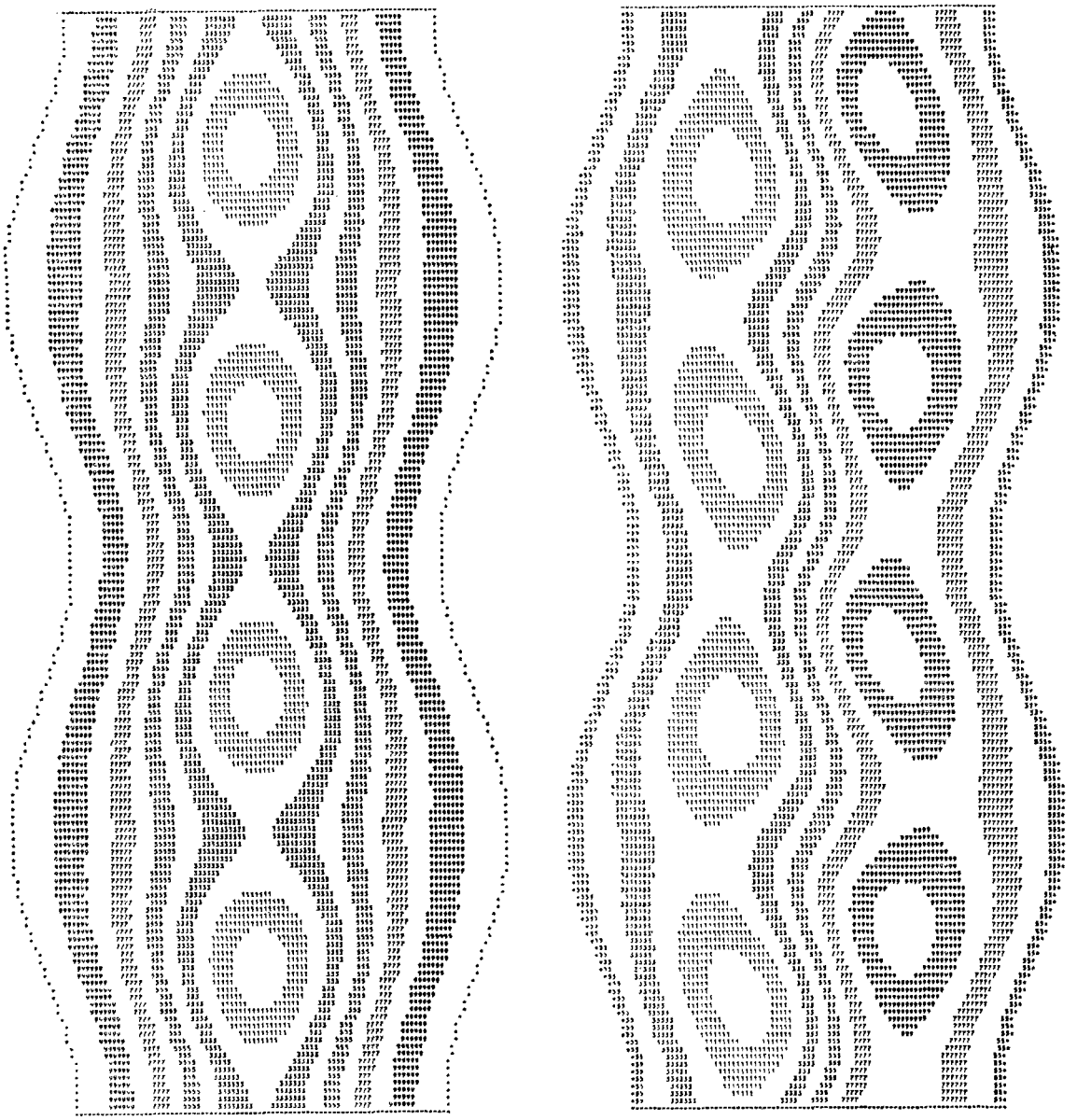

(*a*) (*b*)

FIGURE 4. (*a*) ψ_2 plot and (*b*) θ_2 plot for $\omega = 1{\cdot}5$ and $G = 200$.

Velocity and thermal profiles

Before examining the stream function and temperature distribution it is advantageous to examine the computed perturbations (ψ_1, θ_1) and (ψ_2, θ_2) for, say, $\omega = 1{\cdot}5$ and various G. For convenience all of the plots shown embrace two complete wavelengths of the wall geometry.

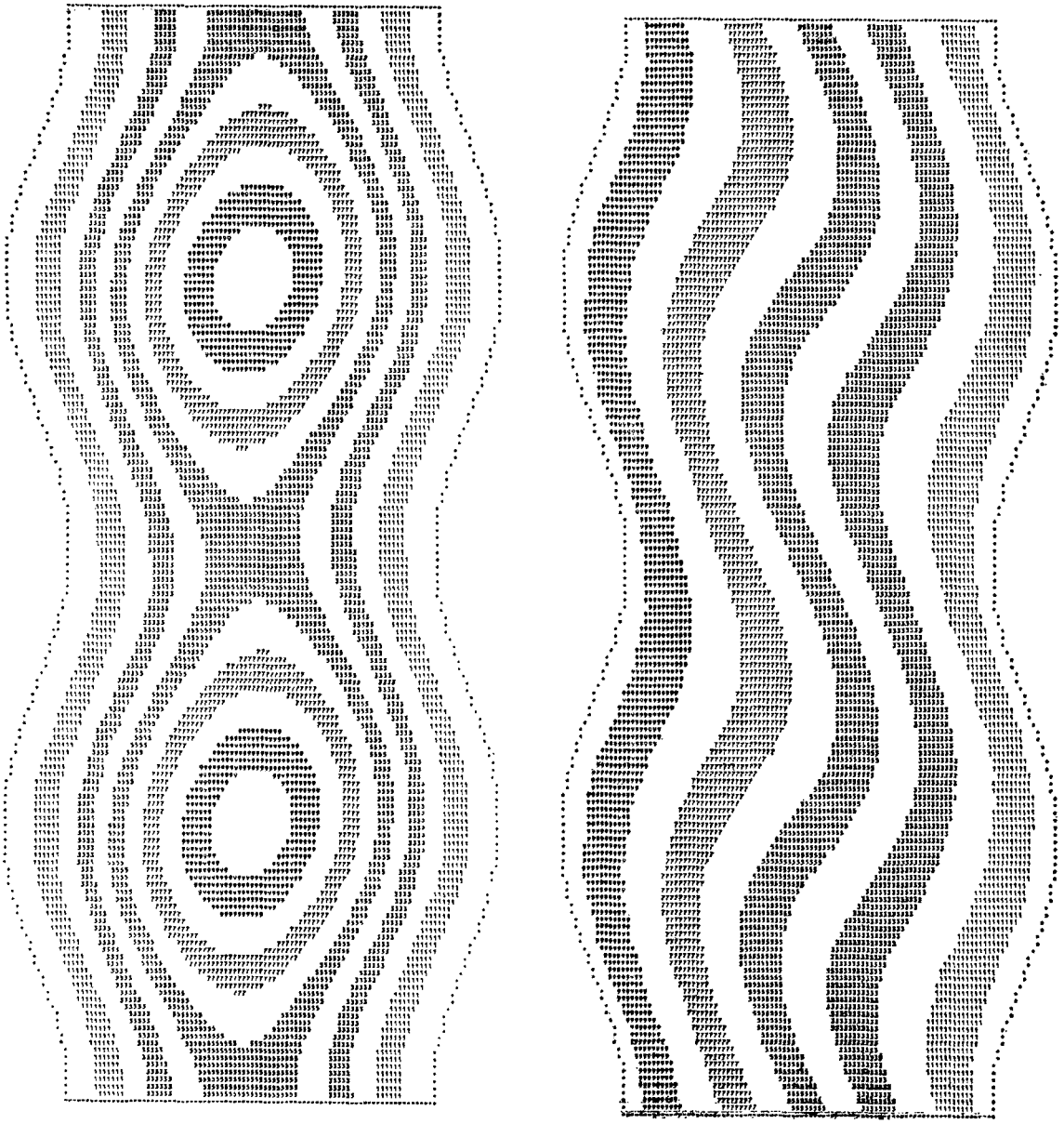

(*a*) (*b*)

FIGURE 5. (*a*) ψ plot and (*b*) θ plot for $\epsilon = 0{\cdot}15$, $\omega = 1{\cdot}5$ and $G = 100$.

The main effect of increasing the Grashof number was found to be one of magnitude, since the shapes of the profiles are nearly identical. The case of $G = 200$ and $\omega = 1{\cdot}5$ is displayed in figures 3 and 4 and in table 2 maximum and minimum values of the perturbation functions are given. It is of interest to mention that the shape of the components ψ_1 and θ_1 in the next mode region

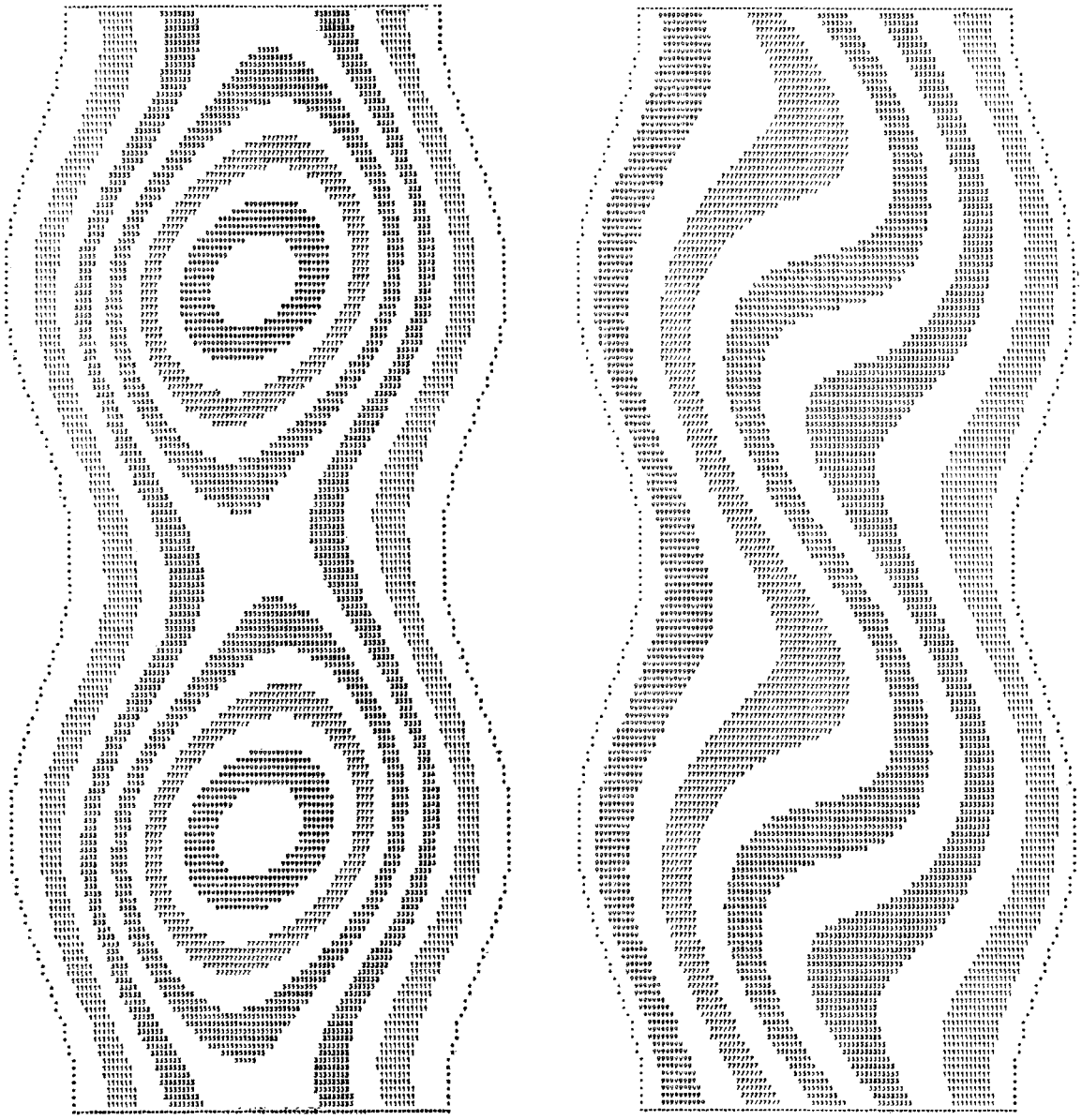

(*a*) (*b*)

FIGURE 6. (*a*) ψ plot and (*b*) θ plot for $\epsilon = 0{\cdot}15$, $\omega = 1{\cdot}5$ and $G = 200$.

($G > 500$) are of the same art form as those displayed, but the relative positions of the maximum and minimum values are interchanged.

In the following isothermals and streamlines are discussed for the typical case $\omega = 1{\cdot}5$ and $\epsilon = 0{\cdot}15$ for various G.

For small G the isothermals will be on contours parallel to the walls, with a slow flow wrapping itself smoothly around the corrugated boundaries. In this case the

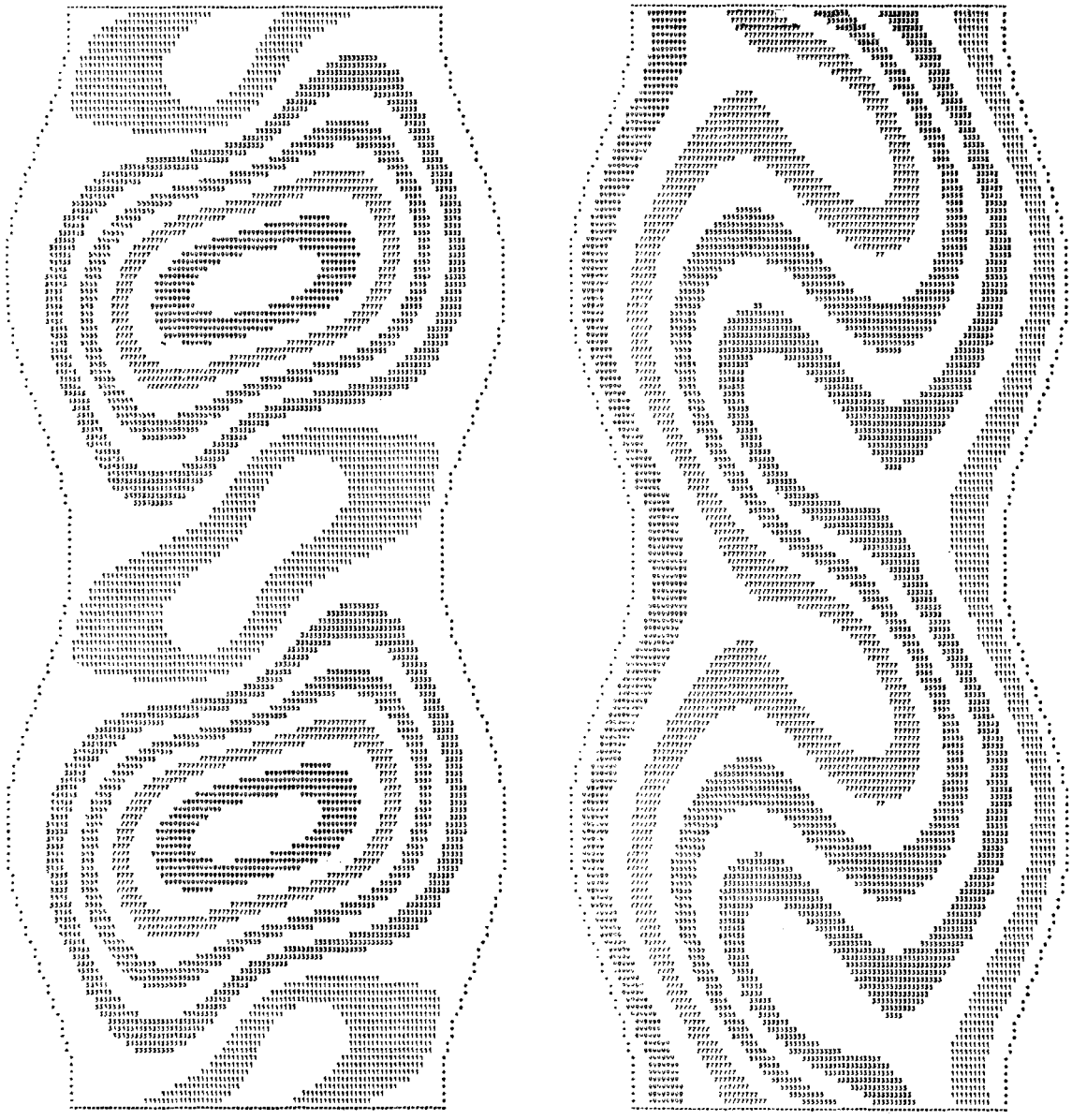

(*a*) (*b*)

FIGURE 7. (*a*) ψ plot and (*b*) θ plot for $\epsilon = 0{\cdot}15$, $\omega = 1{\cdot}5$ and $G = 300$.

mechanism governing the flow and heat transfer is, as in the case of smooth walls, controlled by a balance of the viscous and body forces and heat is transferred by conduction alone.

On increasing the Grashof number the first effects of the protrusions are seen in the appearance of vortices symmetrically placed in the cavity; see for example figure 5 (*a*) for $G = 100$. At this Grashof number heat transfer by convection is still unimportant as seen from figure 5 (*b*).

Plot type / G	ψ_1	θ_1	ψ_2	θ_2
50	±4·29	±0·88	−3·67 0·00	±0·33
100	±8·27	±1·50	−16·71 0·00	±1·36
150	±12·54	±1·95	−43·80 0·00	±2·78
200	±18·03	±2·44	−96·34 0·00	±4·94
250	±26·00	±3·12	−207·1 0·0	±9·00
300	±38·60	±4·19	−486·4 0·0	±17·66

TABLE 2. Maximum and minimum of perturbation functions

As G is further increased, resulting in higher fluid velocities near the walls, the vortex motion becomes more dominant (see figure 6 (*a*) for $G = 200$) and this results in an increase in the role played by convection in the heat-transfer process. The isothermals thus begin to twist, as can be seen clearly from figure 6 (*b*), hot isothermals being displaced towards the cold wall and vice-versa.

It is now clear from figure 7 (*a*), for $G = 300$, that the effects of the curvature of the walls in the vicinity of the neck is to cause the fluid to break away. This results in an almost stagnant region within the fluid which, when driven by the primary vortices, produces a weak secondary vortex. In this region conduction effects, as seen from figure 7 (*b*) clearly predominate. However the isothermals are considerably distorted in the vicinity of the primary vortex leading to marked increases in the wall heat-transfer rates.

It thus appears feasible that, for $G > 300$, further distortion of the isothermals will occur. It is clear from table 2, however, that the convergence of the series (2.14) and (2.15) is doubtful for $G > 300$.

Heat-transfer coefficients

Finally the effects of variation in ω and G on the wall heat flux are examined. Since the thermal field is periodic it is only necessary to consider the integrated heat flux over an area defined by unit width of wall, in a direction perpendicular

to the flow, and over one wavelength $2\pi d/\omega$ of the wall. The integrated heat flux at the wall $\eta = 1$ is defined, for fixed G, by

$$Q_w(\epsilon, \omega) = -K\int_s (\nabla T).d\mathbf{S}, \tag{4.1}$$

where K is the thermal conductivity.

G \ ω	0·50	0·75	1·00	1·25	1·50	1·75	2·00
50	0·878	1·200	1·480	1·666	1·751	1·758	1·725
100	1·741	2·611	3·269	3·638	3·698	3·491	3·127
150	2·842	4·220	5·290	5·967	6·091	5·612	4·732
200	3·978	5·875	7·640	9·065	9·524	8·616	6·772
250	5·095	7·748	10·92	14·15	15·59	13·70	9·760
300	6·235	10·17	16·26	23·98	28·11	23·35	14·40

TABLE 3. Fraction increase in heat flux: values of N_ϵ/ϵ^2

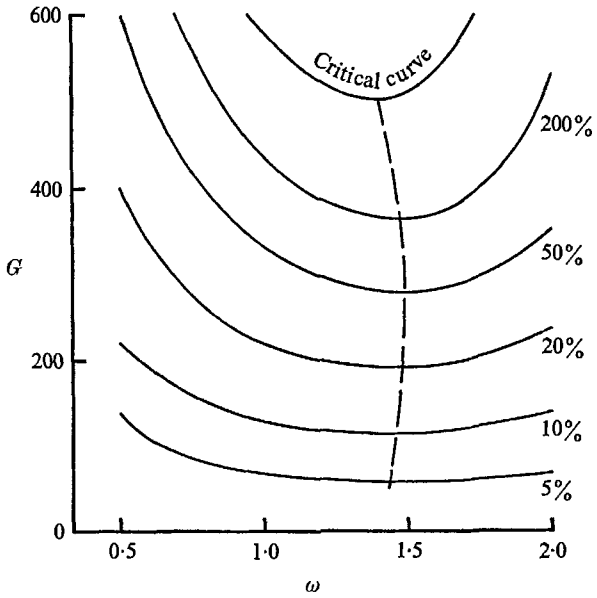

FIGURE 8. Percentage increase in heat transfer for $\epsilon = 0{\cdot}15$.

In terms of the dimensionless variables

$$\frac{Q_w(\epsilon, \omega)}{K(T_1 - T_0)} = \int_0^{2\pi/\omega} \frac{1 + \epsilon^2\omega^2\cos^2(\omega\xi)}{1 + \epsilon\sin(\omega\xi)} \left(\frac{\partial\theta}{\partial\eta}\right)_{\eta=1} d\xi, \tag{4.2}$$

since the wall $\eta = 1$ is an isothermal. Expanding the above in powers of ϵ yields

$$\frac{Q_w(\epsilon, \omega)}{K(T_1 - T_0)} = \frac{2\pi}{\omega}\left[1 + \frac{\epsilon^2}{2}\left(1 + \omega^2 + \left(\frac{dg_1}{d\eta}\right)_1 - 2\left(\frac{dg_3}{d\eta}\right)_1\right) + O(\epsilon^4)\right]. \tag{4.3}$$

The dimensionless number N_ϵ, defined by

$$N_\epsilon = \frac{Q_w(\epsilon,\omega) - Q_w(O,\omega)}{Q_w(O,\omega)} \tag{4.4}$$

is used to compare the heat flux with that for the reference case $\epsilon = 0$ and is the fractional increase in heat flux. Clearly, neglecting terms of order ϵ^4,

$$N_\epsilon = \tfrac{1}{2}\epsilon^2 \left[1 + \omega^2 + \left(\frac{dg_1}{d\eta}\right)_1 - 2\left(\frac{dg_3}{d\eta}\right)_1\right]. \tag{4.5}$$

In table 3 values of N_ϵ/ϵ^2 are given for $G = 50\ (50)\ 300$ and $\omega = 0{\cdot}50\ (0{\cdot}25)\ 2{\cdot}00$. In figure 8 percentage increases in heat transfer are displayed for the case $\epsilon = 0{\cdot}15$.

Considerable changes in the percentage increase in heat transfer may be observed in figure 8, being much more marked for values of G near the critical value. For a given increase in the heat-transfer rate the process of heat transfer between the walls will be most efficient at the lowest possible value of the Grashof number. The optimum values of (ω, G) are thus given by the locus of the minimum of the (ω, G) versus N_ϵ curves. This locus has been indicated in figure 8 by the dashed curve.

One of the authors (A. W.) is indebted to the Science Research Council for a maintenance grant.

REFERENCES

BOUSSINESQ, J. 1903 *Theorie Analytique de la Chaleur*, vol. 2. Paris: Gauthier-Villars.

LANCE, G. N. 1960 *Numerical Methods for High Speed Computers*. London: Iliffe and Sons Ltd.

OSTRACH, S. 1964 In *Theory of Laminar Flows* (ed. F. K. Moore), ch. F4. Oxford University Press.

VEST, C. M. & ARPACI, V. S. 1969 *J. Fluid Mech.* **36**, 1.